Simulation of Impurity Diffusion in a Strained Nanowire Using Off-Lattice KMC

Weidong Guo[1,*], Tim P. Schulze[1] and Weinan E[2]

[1]*Department of Mathematics, University of Tennessee, Knoxville, TN 37996-1300, USA.*
[2]*Department of Mathematics and Program in Applied and Computational Mathematics, Princeton University, Princeton, NJ 08544-1000, USA.*

Abstract. Kinetic Monte Carlo (KMC) is a stochastic model used to simulate crystal growth. However, most KMC models rely on a pre-defined lattice that neglects dislocations, lattice mismatch and strain effects. In this paper, we investigate the use of a 3D off-lattice KMC algorithm. We test this method by investigating impurity diffusion in a strained FCC nanowire. While faster than a molecular dynamics simulation, the most general implementation of off-lattice KMC is much slower than a lattice-based algorithm. An improved procedure is achieved for weakly strained systems by pre-computing approximate saddle point locations based on unstrained lattice structures. In this way, one gives up some of the flexibility of the general method to restore some of the computational speed of lattice-based KMC. In addition to providing an alternative approach to nano-materials simulation, this type of simulation will be useful for testing and calibrating methods that seek to parameterize the variation in the transition rates for lattice-based KMC using continuum modeling.

PACS: 02.70.Rr, 02.70.Uu, 66.30Jt, 66.30Pa

Key words: Off-lattice KMC, nanowire, strain rate, impurity diffusion.

1 Introduction

Kinetic Monte Carlo (KMC) is a stochastic model that simulates the atomic details of crystal growth and evolution using probabilistic rules to govern deposition, diffusion and other transition processes [1]. This technique was first adopted in the early 1970s [2, 3] and had found many uses in surface diffusion on adsorbed mono layers [4], growth of

---

*Corresponding author. *Email addresses:* `gwdtj@yahoo.com` (W. Guo), `schulze@math.utk.edu` (T. P. Schulze), `weinan@math.princeton.edu` (W. E)

polymer crystals [5] and self-organized nanowires [6]. In contrast to the thermodynamic Monte Carlo methods, which aimed at predicting the equilibrium state of molecular systems, KMC seeks to provide information about a system's evolution. In KMC, transition rates between states depend on both the energy of the configuration before hopping, as it would be in other Monte Carlo techniques, and on the energy barrier between the states [7]. The aim of this method is to identify a significant set of possible events to describe the general behavior of evolution processes and to find the energy barrier between the saddle point and local minima for each of these. The principal KMC algorithm is based on the method of Bortz, Kalos and Lebowitz [8] (BKL), which will be introduced in Section 2.

In KMC, all lattice points, energy barriers and diffusion rates are normally defined before computation begins. As a consequence, dislocations, lattice mismatch and strain effects are neglected. A molecular dynamics (MD) simulation can be used for off-lattice simulation, however, it is limited to a time scale on the order of 10^{-6} seconds or less. An off-lattice KMC (OLKMC) simulation can be used for longer simulations while taking into account some elastic effects. Off-lattice KMC will also be useful for testing and calibrating other macroscopic tools, such as schemes that aim to combine continuum modeling with KMC.

Off-lattice simulations themselves can be implemented in a number of ways, with the usual tradeoff between faithful representation of the physical processes and computational speed. At one extreme, Jonsson *et al.* [9] have implemented a method that uses harmonic transition state theory (TST), described below, to estimate transition rates between local minima for the energy landscape in the full *n*-particle configuration space. Further, they make no assumptions about the approximate location of the saddle points separating two energy minima. This represents the most computationally intensive version of OLKMC, where random initial guesses must be used to locate transition points. In this method, locating the set of transition points is the most costly part of the algorithm. Even with parallel implementation this type of calculation is presently limited to a few hundred atoms or less.

An approach which is less computationally intensive, but less accurate, is found in the work of Much *et al.* [10,11] in which an OLKMC algorithm has been developed to simulate the early stage of heteroepitaxial growth for adsorbate layers. A simple *Lennard-Jones* potential is employed in their simulation. The transition points are sought in a "frozen crystal" approximation where only a single atom is moved within the configuration space in order to locate approximate saddle points. This method has been used to simulate surface diffusion during "1+1"-dimensional epitaxial growth and submonolayer "2+1"-dimensional growth growth. The resulting simulation is considerably fast, but still does not approach the computational speed of latticed based simulation and the saddle point problem is again the most intensive part of the algorithm.

Still another approach to incorporating elastic effects into KMC can be found in the works [12–14]. These authors use a model where the transition rate is approximated by using only the binding site energy. The atoms interact through a nearest neighbor net-

work of linear springs and the energy is calculated by using a displacement field relative to a fixed lattice.

In this paper, we investigate an OLKMC method that relies on having approximate saddle point locations, allowing the method to function in three dimensions for a few thousand particles. We consider saddle-point computation using both a relaxation of the full configuration as well as the frozen-crystal approximation in order to assess the reliability of the latter. We also explain a simple improvement over the basic OLKMC algorithm that involves the implementation of *a priori* over- and under-estimates for the transition rates and subsequent rejection of some moves upon calculation of the actual rate. This is reminiscent of other algorithms combining rejection and rejection-free KMC [15].

Our method is motivated by the need to simulate off-lattice phenomena in various nanoscale devices. As a benchmark problem, we examine interstitial diffusion in crystalline nanomaterials. While this is a topic of interest in technological applications [16,17], our interest here is principally to evaluate a particular approach to molecular simulation. Specifically, our prototype problem considers impurity diffusion in a strained FCC nanowire. The rest of this paper is divided into four parts: an explanation of the OLKMC method, the application of the method to our prototype problem, our results and some concluding remarks.

2 Description of method

The total potential energy is modeled by using classical, empirical formulae like the Lennard-Jones potential [18], which is a sum of pair-wise interactions, or the embedded atom potential [19,20]. As it is sufficient to illustrate the method, we primarily focus on the Lennard-Jones potential:

$$\Phi = \sum_{ij} \Phi_{ij} = 4U_a \sum_{ij} \left[\left(\frac{\sigma}{d_{ij}} \right)^{12} - \left(\frac{\sigma}{d_{ij}} \right)^{6} \right], \tag{2.1}$$

where U_a represents the depth of the energy well that an atom in equilibrium resides in, σ represents a length scale for the mean particle separation in equilibrium and d_{ij} is the distance between particles i and j. Scaling lengths with the equilibrium particle separation σ, we then take $\sigma_a = 1$ for the primary crystal, along with $U_a = 0.15$ ev for the depth of the energy well.

The potential energy landscape contains an enormous number of local minima in the 3N-dimensional configuration space consisting of the particle position vectors $\mathbf{x}_i \in \mathbb{R}^3$. These local minima serve as the temporary resting places of particles in the zero-temperature approximation and, more generally, as approximate locations of the basins of attraction for particle positions in low-temperature, solid-phase materials. In a corresponding molecular dynamics simulation, all of the particles will undergo Brownian-like

motions that are largely localized within these basins, but also feature infrequent transitions where the system moves from one basin (local minimum) to a neighboring minimum in the configuration space. According to transition state theory [21], the rate at which these transitions are made is related to the energy barrier that must be overcome by crossing the saddle-points that separate neighboring local minima.

In a general solid-phase material with grain boundaries, dislocations and irregular surface structure, there will be an undetermined number of near-by saddle points associated with a given local minimum. We limit our model to transitions involving a single impurity atom diffusing in the interstices of a strained lattice. While not all likely transition pathways will be detected by this procedure—concerted moves of impurity clusters, for example—intuition suggests that most will and that it is one of the simplest ways to efficiently address large configurations. To further enhance computational performance, we employ a cut-off length σ_c, so that if $d_{ij} > \sigma_c$ we ignore the contribution of the term Φ_{ij} to the total potential Eq. (2.1). In this paper, the cut-off is normally chosen to be three times the mean particle separation.

With these two approximations in place, the OLKMC method reduces to a combination of optimization and the standard algorithms for KMC. From an optimization perspective, there are two types of problems involved. First, the material must be relaxed within the configuration space to its local minimum. For each attempted event, a second calculation must then be made to determine the saddle-point energy. In this paper, all optimization is performed by using a nonlinear conjugate gradient algorithm along with accurate initial guesses derived from a perfect lattice that improve convergence and avoid numerical instabilities. For the local minima we minimize the energy directly; for the saddle-points we minimize $|\nabla\Phi|^2$. Both absolute and relative convergence criteria are employed. We use the maximum norm of the potential (or $|\nabla\Phi|^2$ for saddle points) for the absolute convergence criteria and the maximum norm of the displacement vector for relative convergence. Computationally, this is still an enormously expensive task with limited feasibility unless further approximations are made. To this end, we also explore focusing the relaxation algorithm on a subset of the particles surrounding the particle making a transition. In its most extreme form, this reduces to the frozen crystal approximation mentioned above.

In its simplest form, the KMC can be implemented in an entirely rejection-free manner, following the standard BKL [8] algorithm. Initially the rates for all events r_n are initially calculated using harmonic transition state theory [21]

$$r_n(\Delta\Phi, T) = k_0 \exp -\left(\frac{\Delta\Phi}{k_B T}\right), \tag{2.2}$$

where $\Delta\Phi$ represents the energy barrier between the transition state and the binding state. Here, T denotes the temperature, k_B is the Boltzmann constant and k_0 is the attempt frequency. To select one event among the many possibilities, the sum of the transition rates, $S_N = \sum_{n=1}^{N} r_n$, is computed, retaining the partial sums S_n. A random number $r \in [0, S_N)$ is then selected and one searches through the list of events until $r < S_n$. For lattice-

based KMC, it is important to make this search efficient, but the search represents a very small part of the computation for OLKMC. Following standard KMC practice, the time interval between two events can then be selected randomly from a Poisson distribution $\Delta t = -\log(u)/S_N$, where $u \in [0,1)$ is a uniformly distributed random number.

In the present situation, the extremely high cost of evaluating the transition and binding state energies, along with the relatively well-structured environment of a weakly strained lattice, suggests augmenting this procedure with reliable under- ($\check{r}_n \leq r_n$) and over- ($\hat{r}_n \geq r_n$) estimates of the actual rates. The over-estimates allow one to restrict the expensive update calculations to the event that is actually selected, at the small cost of sometimes rejecting a move. To implement this, replace the sum of rates with the overestimate $\hat{S}_N = \sum_{n=1}^{N} \hat{r}_n$ and proceed as before. After a candidate has been selected, calculate the true rate r_n and compare the selected random number r with the revised partial sum $\hat{S}_{n-1} + r_n$ to determine whether or not the event should be rejected. In either case, the time should be advanced using over-estimated rates. An accepted event is realized by moving this atom to the approximate location of its new position where it will be re-relaxed at some later point in the simulation. If a reliable under-estimate is also available, one can avoid the optimization calculations on many of the iterations by also comparing the selected random number r with the underestimate $\hat{S}_{n-1} + \check{r}_n$. If r falls short of this number, one can execute the event without checking for rejection, thus avoiding the actual rate calculation.

3   Impurity diffusion in a strained FCC nanowire

As a prototype problem, we test the algorithm in the context of impurity diffusion in a strained FCC nanowire. Fig. 1(a) shows an FCC unit cell which can be decomposed into one octahedral section and eight tetrahedral sections, as suggested by Fig. 1(b). If the repulsive interaction between the impurity and the lattice particles is tuned appropriately, the impurity particles will occupy local minima at the centers of these polyhedral regions, as shown in Fig. 1(b). We use the perfect FCC lattice to generate initial guesses for the local minima and saddle points of a strained lattice. This allows us to efficiently simulate the interstitial diffusion of impurities in weakly strained crystals.

The ideal FCC lattice can be defined using integer combinations of three basis vectors

$$\mathbf{a} = \frac{\hat{\mathbf{i}} + \hat{\mathbf{j}}}{\sqrt{2}} \times a_e \quad \mathbf{b} = \frac{\hat{\mathbf{i}} + \hat{\mathbf{k}}}{\sqrt{2}} \times a_e \quad \mathbf{c} = \frac{\hat{\mathbf{k}} + \hat{\mathbf{j}}}{\sqrt{2}} \times a_e, \tag{3.1}$$

where $a_e = \sqrt[6]{2}\sigma_a$ is the equilibrium distance between two atoms in an isolated environment. An arbitrary lattice point can be defined by $\mathbf{v} = n_1\mathbf{a} + n_2\mathbf{b} + n_3\mathbf{c}$. As shown in Fig. 2, we define the nanowire geometry by orientating the axis parallel to a unit vector $\hat{\mathbf{n}}$, chosen orthogonal to a faceting direction, and include in the initial wire all lattice points $\mathbf{v}$ satisfying

$$|\mathbf{v} \cdot \hat{\mathbf{n}}| \leq L, \tag{3.2a}$$

$$|\mathbf{v} - (\mathbf{v} \cdot \hat{\mathbf{n}})\hat{\mathbf{n}}| \le R, \tag{3.2b}$$

where L and R are the length and radius of the nanowire respectively. Each local energy minimum has a number of saddle points associated with it. Figs. 3(a) and 3(b) show octahedral (O) and tetrahedral (T) sites, respectively, where the small spheres at the center of each face represent near-by saddle points while the large spheres represent the local minima. For an O-site, there are eight saddle points while there are four for a tetrahedron. In the search for the location of saddle points in a strained system, initial guesses can be based on these ideal structures. For example, when an impurity rests in an O-site, the initial guesses are

$$\mathbf{x} = \mathbf{x}_{eq} + d_O \times \mathbf{e_i}^T, i \in \{1, 2, \dots, 8\}, \tag{3.3}$$

where $\mathbf{x}_{eq} \in \mathbb{R}^3$ is a local minimum. The distance between the local minimum and the saddle point is d_O and $\{\mathbf{e}_i\}$ is a set of eight unit vectors pointing in the direction of the initial guesses

$$\begin{pmatrix} \mathbf{e_1} \\ \mathbf{e_2} \\ \mathbf{e_3} \\ \mathbf{e_4} \\ \mathbf{e_5} \\ \mathbf{e_6} \\ \mathbf{e_7} \\ \mathbf{e_8} \end{pmatrix} = \frac{1}{\sqrt{3}} \begin{pmatrix} 1 & 1 & 1 \\ -1 & -1 & 1 \\ 1 & 1 & -1 \\ -1 & -1 & -1 \\ 1 & -1 & 1 \\ -1 & 1 & 1 \\ 1 & -1 & -1 \\ -1 & 1 & -1 \end{pmatrix}. \tag{3.4}$$

The distance d_O can be expressed in terms of a_e based on the geometry of an octahedron

$$d_O = \frac{\sqrt{6}a_e}{6}. \tag{3.5}$$

For a T-site, the initial guesses are

$$\mathbf{x} = \mathbf{x_{eq}} + d_T \times \mathbf{e_{ij}}^T, \ i \in \{1, 2, \dots, 8\} \ j \in \{1, 2, 3, 4\}, \tag{3.6}$$

where d_T is the distance between the local minima and saddle point

$$d_T = \frac{(5\sqrt{6} - 3\sqrt{10})a_e}{15}. \tag{3.7}$$

As indicated by in Fig. 1(b), an O-site is adjacent to eight T-sites, each having a distinct orientation. The set of initial guesses can be formed from the same guesses $\{\mathbf{e}_i\}$ used in the octahedral case, but must be indexed by both the eight possible tetrahedral orientations and the four faces of each tetrahedron. Thus, $\mathbf{e_{ij}} \in \mathbb{R}^3$ represents an initial guess for

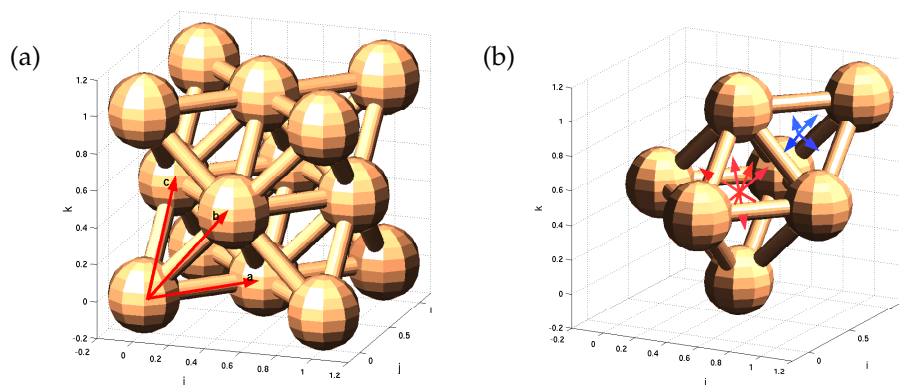(a)   (b)

Figure 1: FCC unit cell composed of one octahedral section and eight tetrahedral sections. (a) FCC unit cell and (b) Decomposition of FCC unit cell.
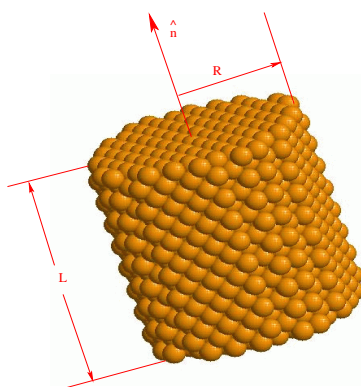

Figure 2: FCC nanowire with its axis parallel to a unit vector $\hat{\mathbf{n}}$, chosen orthogonal to a faceting direction. Here, L and R are the length and radius of the nanowire, respectively.
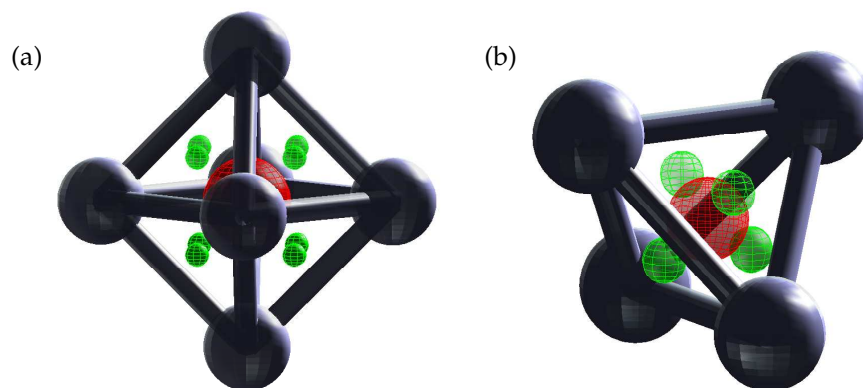
(a)   (b)

Figure 3: Illustration of local minima and corresponding saddle points. The small spheres at the center of each face represent near-by saddle points while the larger spheres represent the local minima. (a) Octahedron and (b) Tetrahedron.

the ith orientation and the j face:

$$
\begin{pmatrix}
e_{11} & e_{12} & e_{13} & e_{14} \\
e_{21} & e_{22} & e_{23} & e_{24} \\
e_{31} & e_{32} & e_{33} & e_{34} \\
e_{41} & e_{42} & e_{43} & e_{44} \\
e_{51} & e_{52} & e_{53} & e_{54} \\
e_{61} & e_{62} & e_{63} & e_{64} \\
e_{71} & e_{72} & e_{73} & e_{74} \\
e_{81} & e_{82} & e_{83} & e_{84}
\end{pmatrix}
=
\begin{pmatrix}
e_3 & e_4 & e_5 & e_6 \\
e_3 & e_4 & e_5 & e_6 \\
e_1 & e_2 & e_7 & e_8 \\
e_1 & e_2 & e_7 & e_8 \\
e_1 & e_2 & e_7 & e_8 \\
e_1 & e_2 & e_7 & e_8 \\
e_3 & e_4 & e_5 & e_6 \\
e_3 & e_4 & e_5 & e_6
\end{pmatrix} .
\tag{3.8}
$$

Here the faces of the tetrahedron have been labelled so that each row in the matrix on the right-hand side is repeated four times.

For these initial guesses to be valid, the impurity must interact relatively weak with the primary crystal, so that the FCC structure remains intact. Also, the equilibrium separation between an impurity and a lattice particle must be larger than the distance separating the central point in the O- or T-sites from the centers of their respective faces. If the latter condition is not met, there will be a different local minima structure for impurity locations where local minima are associated with each undeformed lattice site in a sattlelight configuration. With these considerations in mind, we model the interaction of the impurity with the primary material forming the lattice using a Lennard Jones potential (2.1) with different material parameters. For interactions between impurities, we use the values $U_b = 0.1$ ev and $\sigma_b = 0.4\sigma_a$. The interaction between a nanowire particle and an impurity is defined by $U_{ab} = \sqrt{U_a U_b}$ and $\sigma_{ab} = (\sigma_a + \sigma_b)/2$.

To simulate impurity diffusion in strained nanowires, we first uniformly stretch or compress the wire by transforming the axial coordinate $z \to (1+\epsilon)z$ and then relax the transformed configuration to the local minimum that this approximates while constraining the layers of atoms at the ends of the nanowire. We assume all impurities evaporate once they reach the nanowire wall.

4   Results

We begin by illustrating diffusion of a single impurity in a statically strained nanowire. Figs. 4(a) and 4(b) show a sample path that demonstrates the detailed trajectory of one impurity diffusing from the central point to the boundary of a nanowire. The impurity alternately diffuses through the adjacent O- and T-sites. The binding energy in T-sites is higher than O-sites, so that the impurity binds preferentially in the O-sites and, on average, the time intervals spent in these sites are much longer than in the T-sites. This is consistent with one's intuition and in agreement with the existing theory [16].

Fig. 5 illustrates a simulation with multiple impurities diffusing simultaneously. Several O-sites are randomly selected as initial impurity locations. In the case when adjacent O and T-sites are occupied, the number of saddle points is less than eight in an O-site and
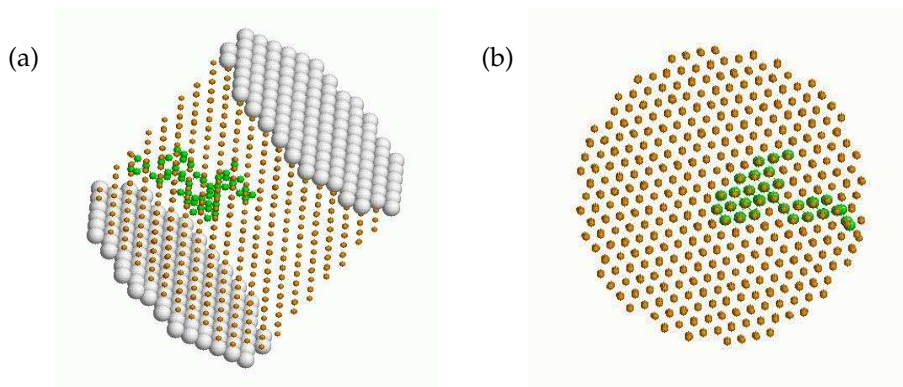
Figure 4: Sample path of impurity diffusion. (a) Sample path and (b) Side view of sample path.
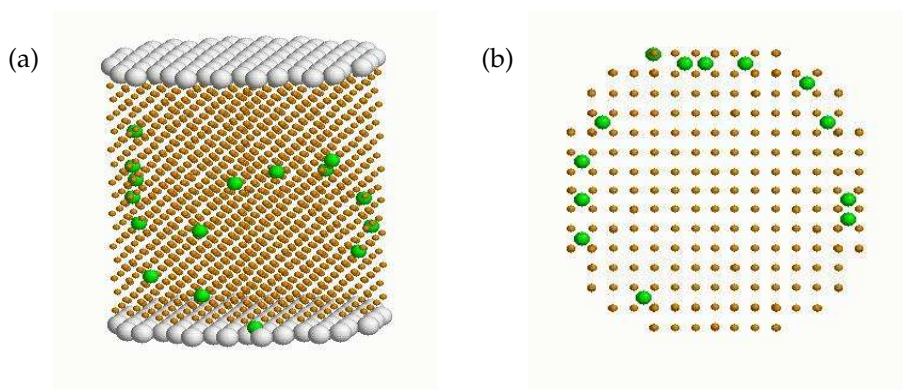

Figure 5: Diffusion of multiple impurities. (a) Final positions of multiple impurities and (b) Top view of multiple impurities.

less than four in a T-site. Figs. 5(a) and 5(b) show both the side and top view of the final position distribution for a simulation with multiple impurities.

To test our code and as a step toward building a faster lattice-based KMC that accounts for elastic effects using tabulated rates and interpolation, we have collected a number of energy barriers in Table 1 using a relaxation scheme that does not rely on any form of the frozen crystal approximation. The table shows the energy barriers for a single adatom in a central O or T site diffusing in each of the eight possible directions defined in Eq. (3.4) with 1% and 2% strain along the three principal faceting directions 100,110 and 111. The unstrained numbers are 0.833 ev for an O-site and 0.125 ev for a T-site. Note that the rates for a given axis orientation come in groups that are consistent with the symmetry of the given axis. To evaluate the extent to which the frozen crystal approximation can be relied upon, we have also collected these energy barriers using an approximation (Table 2) where the potential energy landscape is probed for saddle points by moving only a single atom at a time. It is clear from the comparison that neglecting the distortion of the crystal around the hopping atom tends to give a much higher energy

Table 1: This table shows the energy barriers for a single adatom in a central O and T site diffusing in each of the eight possible directions defined in (3.4) with 1% and 2% strain along the three principal faceting directions 100,110 and 111. The total number of atoms in the nanowire for the 100, 110 and 111 cases is 946, 990 and 1012, respectively. The data for Table 1 was calculated by relaxing the full system.

	1%						2%					
	100		110		111		100		110		111	
	O	T	O	T	O	T	O	T	O	T	O	T
e_1	0.810	0.124	0.820	0.140	0.860	0.197	0.790	0.119	0.820	0.161	0.880	0.249
e_2	0.810	0.124	0.820	0.140	0.770	0.103	0.790	0.119	0.820	0.161	0.730	0.089
e_3	0.810	0.124	0.820	0.140	0.770	0.103	0.790	0.119	0.820	0.161	0.770	0.103
e_4	0.810	0.124	0.820	0.140	0.860	0.197	0.790	0.119	0.820	0.161	0.880	0.249
e_5	0.810	0.124	0.790	0.110	0.770	0.103	0.790	0.119	0.740	0.086	0.730	0.089
e_6	0.810	0.124	0.790	0.110	0.770	0.103	0.790	0.119	0.740	0.086	0.730	0.089
e_7	0.810	0.124	0.790	0.110	0.770	0.103	0.790	0.119	0.740	0.086	0.730	0.089
e_8	0.810	0.124	0.790	0.110	0.770	0.103	0.790	0.119	0.740	0.086	0.730	0.089

Table 2: This table shows the energy barriers, calculated using the frozen crystal approximation, for a single adatom in a central O and T site diffusing in each of the eight possible directions defined in (3.4) with 1% and 2% strain along the three principal faceting directions 100, 110 and 111. The total number of atoms in the nanowire for the 100, 110 and 111 cases is 946, 990 and 1012, respectively.

	1%						2%					
	100		110		111		100		110		111	
	O	T	O	T	O	T	O	T	O	T	O	T
e_1	2.780	0.520	2.813	0.592	2.983	0.848	2.720	0.510	2.832	0.698	3.069	1.092
e_2	2.780	0.520	2.813	0.592	2.641	0.425	2.720	0.510	2.832	0.698	2.505	0.363
e_3	2.780	0.520	2.813	0.592	2.641	0.425	2.720	0.510	2.832	0.698	2.505	0.363
e_4	2.780	0.520	2.813	0.592	2.983	0.848	2.720	0.510	2.832	0.698	3.069	1.092
e_5	2.780	0.520	2.695	0.451	2.641	0.425	2.720	0.510	2.566	0.356	2.505	0.363
e_6	2.780	0.520	2.695	0.451	2.641	0.425	2.720	0.510	2.566	0.356	2.505	0.363
e_7	2.780	0.520	2.695	0.451	2.641	0.425	2.720	0.510	2.566	0.356	2.505	0.363
e_8	2.780	0.520	2.695	0.451	2.641	0.425	2.720	0.510	2.566	0.356	2.505	0.363

barrier in the case of interstitial diffusion.

Next we explore the possibility of using some intermediate type of frozen crystal approximation by constraining all but a limited set of atoms in the vicinity of the hopping atom. These results are shown in Figs. 6(a) and 6(b), where we plot the energy barrier value obtained as a function of the number of unconstrained neighbors in the calculation. Figs. 6(a) and 6(b) show that one can obtain about 95% accuracy for an O-site by relaxing 50 unconstrained neighbors and 92% accuracy for a T-site using 100 unconstrained neighbors. Below, we shall use this level of accuracy, which corresponds to a constrained-neighbor cut-off radius of $r = 3a_e$, to calculate energy barriers under various
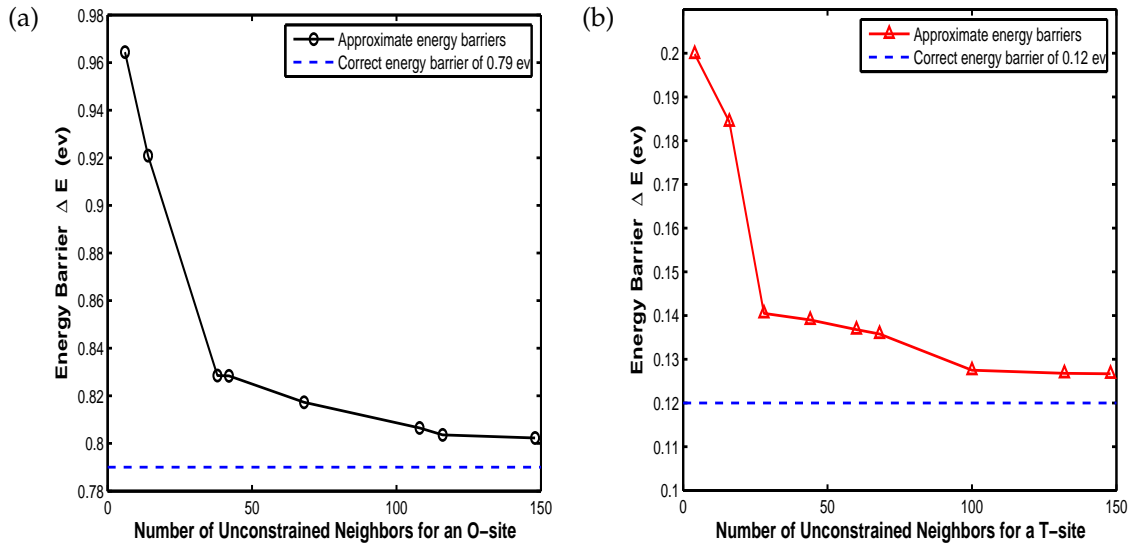
Figure 6: A plot of the energy barrier obtained as a function of the number of unconstrained neighbors for an O-site and T-site at the center of a wire under 2% strain and oriented perpendicular to the {100} facet.
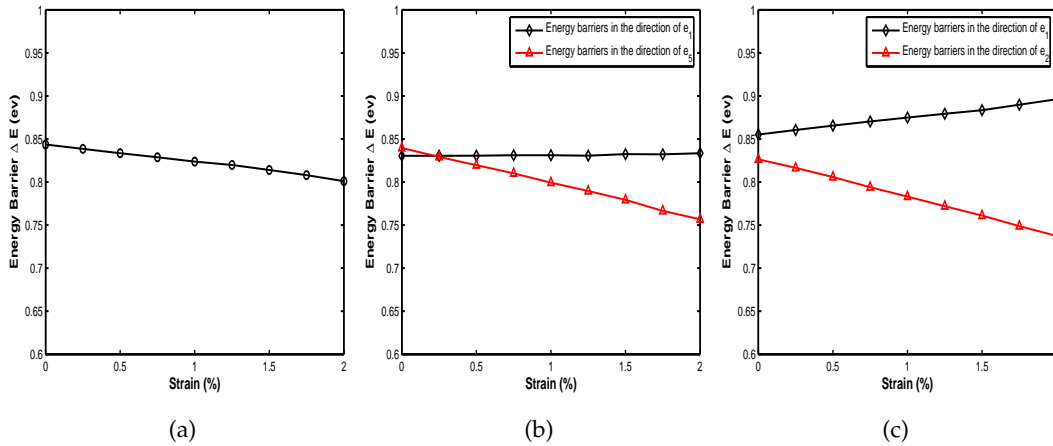

Figure 7: A plot of the energy barrier versus strain for an O-site at the center of wires with different orientations. The calculations use a frozen crystal approximation with an unconstrained-neighbor cut-off distance $r = 3\sigma_a$. (a) Stretching in the 100 direction, (b) Stretching in the 110 direction and (c) Stretching in the 111 direction.

states of stress.

In Figs. 7(a)-7(c) we consider the influence of uniaxial stretching on interstial diffusion. We find that the hopping rate for a single atom is increased in some directions and decreased in others when the nanowire is stretched. For instance, stretching the nanowire along the 100 direction will uniformly decrease the energy barrier for each of the eight possible directions defined in Eq. (3.4). Stretching along the 111 direction, however, gives
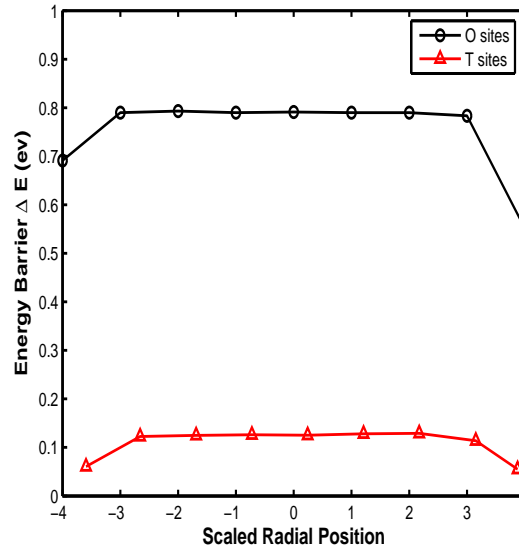
Figure 8: A plot of the energy barrier as a function distance from the center of the nanowire for an O-site and T-site lying in a central cross-section a wire under 2% strain and oriented perpendicular to the {100} facet.

rise to an increase in energy barrier for the $\mathbf{e_1}$ (or geometrically equivalent) direction and a decrease in energy barrier for $\mathbf{e_2}$ (or geometrically equivalent) direction. When stretched along 110 direction, the energy barriers are decreased for the $\mathbf{e_5}$ direction while there is almost no changes for the $\mathbf{e_1}$ direction. Since both T-sites and O-sites show the same trends for energy barrier variation versus strain, only energy barriers for an O-site are plotted.

Finally, as shown in Fig. 8, the energy barriers are relatively uniform in the interior of the uniformly stretched wire. Hence, one can correct the energy barrier by adding a constant to it in order to employ the frozen crystal method. There are, however, significant variations as one approaches the surface of the wire. This type of surface effect is especially important in heteroepitaxy. Our results suggest the possibility of a hybrid simulation that combines lattice-based KMC in the interior and off-lattice KMC near the surface. Unlike the present implementation, however, it is extremely difficult to anticipate the approximate location of transition points near surfaces due to reconstruction, especially for strained surfaces.

5   Conclusion

We have implemented a 3D OLKMC algorithm capable of simulating off-lattice phenomena in various nanodevices. This method differs from previous off-lattice work in that it is aimed at weakly strained systems where the lattice geometry can provide good initial guesses for transition points. In order to demonstrate the method, we examined a

strained FCC nanowire using a Lennard-Jones potential. We explored the possibility of some type of frozen crystal approximation and found that although neglecting the local distortion of the crystal gives rise to a much higher energy barrier, one can still employ some forms of frozen crystal approximation by either adding a correction to the energy barrier or by using a larger set of unconstrained atoms. Our simulations showed that the hopping rate for an adatom is not uniformly altered by a macroscopic strain, but is dependent on the stretching direction as well as the hopping direction of an adatom. We provided evidence that suggests rates in regions of the crystals with a slowly varying elastic field could be computed on a coarsenned length-scale and tabulated for use in a lattice-based approach in these regions.

Acknowledgments

References

[1] A. C. Levi, M. Kotrla, J. Phys.-Condens. Mat. 9 (1997) 299.
[2] F. F. Abraham, G. W. White, J. Appl. Phys. 41 (1970) 1841.
[3] G. H. Gilmer, P. Bennema, J. Appl. Phys. 43 (1972) 1347.
[4] C. Uebing, R. Gomer, Surf. Sci. 306 (1994) 419.
[5] J. K. Doye, D. Frenkel, J. Chem. Phys. 110 (1999) 2692.
[6] C. Girardet, C. Ramseyer, F. Picaud, Physica Scripta 68 (2003) C104.
[7] D. P. Landau, K. Binder, A Guide to Monte Carlo Simulations in Statistical Physics, Cambridge, New York, 2000.
[8] A. B. Bortz, M. H. Kalos, J. L. Lebowitz, J. Comput. Phys. 17 (1975) 10.
[9] H. Jonsson, G. Henkelman, B. Uberuaga, J. Chem. Phys. 115 (2001) 9657.
[10] F. Much, M. Ahr, M. Biehl, W. Kinzel, Comp. Phys. Comm. 147 (2002) 226.
[11] T. Volkmann, F. Much, M. Biehl, M. Kotrla, Surf. Sci. 586 (2005) 157.
[12] C. H. Lam, C. K. Lee, L. M. Sander, Phys. Rev. Lett. 89 (2002) 216102.
[13] G. Russo, P. Smereka, J. Comp. Phys. 214 (2006) 809.
[14] G. Russo, P. Smereka, SIAM MMS., accepted.
[15] J. P. Devita, L. M. Sander, P. Smereka, Phys. Rev. B., accepted.
[16] B. P. Uberuaga, A. F. Voter, K. K. Sieber, D. S. Sholl, Phys. Rev. Lett. 91 (2003) 105901.
[17] S. C. Hendy, N. J. Laycock, M. P. Ryan, J. Electrochem. Soc. 152 (2005) 8.
[18] S. M. Walas, Phase Equilibria in Chemical Engineering, Butterworth-Heinemann, Newton MA, 1985.
[19] F. Ercolessi, M. Parrinello, E. Tosatti, Philos. Mag. A 58 (1988) 213.
[20] R. J. Wolf, K. A. Mansour, M. W. Lee, Phys. Rev. B 46 (1992) 8027.
[21] D. Frenkel, B. Smit, Understanding Molecular Simulation From Algorithms to Applications, Academic, New York, 2002.
[22] M. Schroeder, D. E. Wolf, Surf. Sci. 375 (1997) 129.
[23] H. Spjut, D. A. Faux, Surf. Sci. 306 (1994) 233.